Freely suspended nanocomposite membranes as highly sensitive sensors

CHAOYANG JIANG, SERGIY MARKUTSYA, YURI PIKUS AND VLADIMIR V. TSUKRUK*

Department of Materials Science and Engineering, Iowa State University, Ames, Iowa 50011, USA
* e-mail: vladimir@iastate.edu

Published online: 26 September 2004; doi:10.1038/nmat1212

Highly sensitive sensor arrays are in high demand for prospective applications in remote sensing and imaging. Measuring microscopic deflections of compliant micromembranes and cantilevers is developing into one of the most versatile approaches for thermal, acoustic and chemical sensing. Here, we report on an innovative fabrication of compliant nanocomposite membranes with nanoscale thickness showing extraordinary sensitivity and dynamic range, which makes them candidates for a new generation of membrane-based sensor arrays. These nanomembranes with a thickness of 25–70 nm, which can be freely suspended over large (hundred micrometres) openings are fabricated with molecular precision by time-efficient, spin-assisted layer-by-layer assembly. They are designed as multilayered molecular composites made of a combination of polymeric monolayers and a metal nanoparticle intralayer. We demonstrate that these nanocomposite membranes possess unparalleled sensitivity and a unique autorecovering ability. The membrane nanostructure that is responsible for these outstanding properties combines multilayered polymer/nanoparticle organization, high polymer-chain orientation, and a pre-stretched state.

Miniature, uncooled sensor arrays are in high demand for cutting edge, prospective applications in remote sensing and imaging. Ultrathin, flexible membranes and microcantilevers are emerging as critical elements in various sensing devices, such as acoustic, chemical, pressure and thermal sensors[1]. To provide high sensitivity (large deflection for low forces) rigid membranes usually manufactured from silicon, ceramic, carbon, and even diamond must have large lateral dimensions (millimetres–centimetres) and microscopic thickness[2–5]. However, the current technology shows severe limitations when significant miniaturization is required for device fabrication, for example, high-resolution sensor imaging arrays with microscopic dimensions of a single pixel. Micromachining and lithography technologies have made it possible to fabricate thin (below 1 μm) inorganic membranes for use as thermal sensors with lateral dimensions close to 1 × 1 mm and with thermal sensitivities around 20 mK (refs 6, 7). However, reducing the lateral dimensions of sensing membranes from this size to the required microscopic range (for example, 100 μm across) drastically increases their flexural rigidity, an occurrence that cannot be compensated for simply by reducing the membrane's thickness. Furthermore, attempts to fabricate highly compliant membranes from polymers, liquid crystals, and lipids have been not very successful to date, producing instead films that are too fragile to sustain significant mechanical stress or changing environment[8–12]. Therefore, the miniaturization of sensors from the microscale to nanoscale faces enormous challenges using the technology available.

Here we report on an innovative fabrication of compliant, robust, lightweight, nanocomposite membranes with extraordinary sensitivity and dynamic range. These nanoscale membranes with a thickness of 25–70 nm, which can be freely suspended over microscopic openings, are fabricated with molecular precision by time-efficient, spin-assisted layer-by-layer assembly (SA-LbL) on a sacrificial substrate. They are designed as multilayered nanocomposites fabricated of precisely assembled polymeric monolayers and metal nanoparticle intralayer. Moreover, we demonstrate that nanocomposite membranes, with nanoscale thickness and microscopic lateral dimensions, can possess unparalleled sensitivity combined with extreme robustness. We believe that these compliant and highly sensitive nanomembranes are a breakthrough for applications in membrane-based microsensor technology.

Conventional LbL assembly is well known as a new technology for the fabrication of sophisticated multilayered nanocomposite materials[13–16]. In our approach, we use the recently introduced SA-LbL

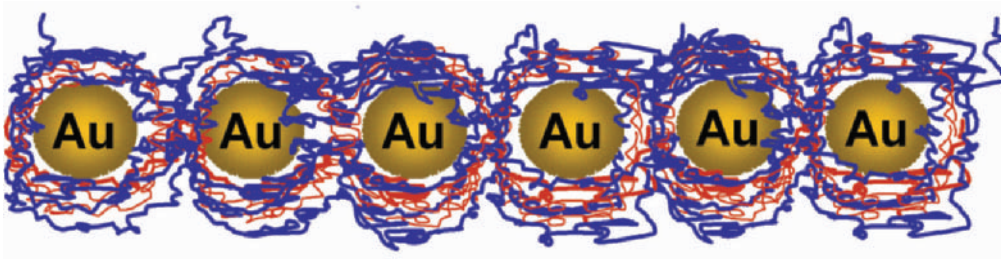

Figure 1 A model of microstructure of the nanocomposite membrane with a gold nanoparticle central layer sandwiched between three polymer bilayers. Adapted from ref. 22; copyright Wiley-VCH 2003.

assembly, which combines the well-known LbL assembly with spin coating (see Supplementary Information)[17–19]. We applied this technology, in conjunction with a sacrificial layer approach[20,21], to fabricate nanocomposite membranes suspended over micromanufactured openings with lateral dimensions of several hundred micrometres and thicknesses of several tens of nanometres as was discussed in detail elsewhere[22] (see Methods). These membranes are composed of a central layer containing gold nanoparticles (12.7 nm in diameter) sandwiched between multilayered films composed of alternating monolayers of two polyelectrolytes, poly(allylamine hydrochloride) (PAH) and poly(sodium 4-styrenesulphonate) (PSS) (Fig. 1, see Supplementary Information and Methods). The general formula for these films is $(PAH\text{-}PSS)_n PAH/Au/(PAH\text{-}PSS)_n PAH$ where n is the number of polyelectrolyte bilayers varying from 3 to 11, or more briefly, nGn (Fig. 1). For this report, we selected membranes with $n = 9$: the 9G9 (55 nm thickness) membrane with a gold nanoparticle central layer and 9_9 (35 nm thickness) membrane, which does not have gold nanoparticles. The results for other membranes will be reported elsewhere. A variation of membrane thicknesses with a number of bilayers is presented in Fig. 2a with arrows marking a choice for this

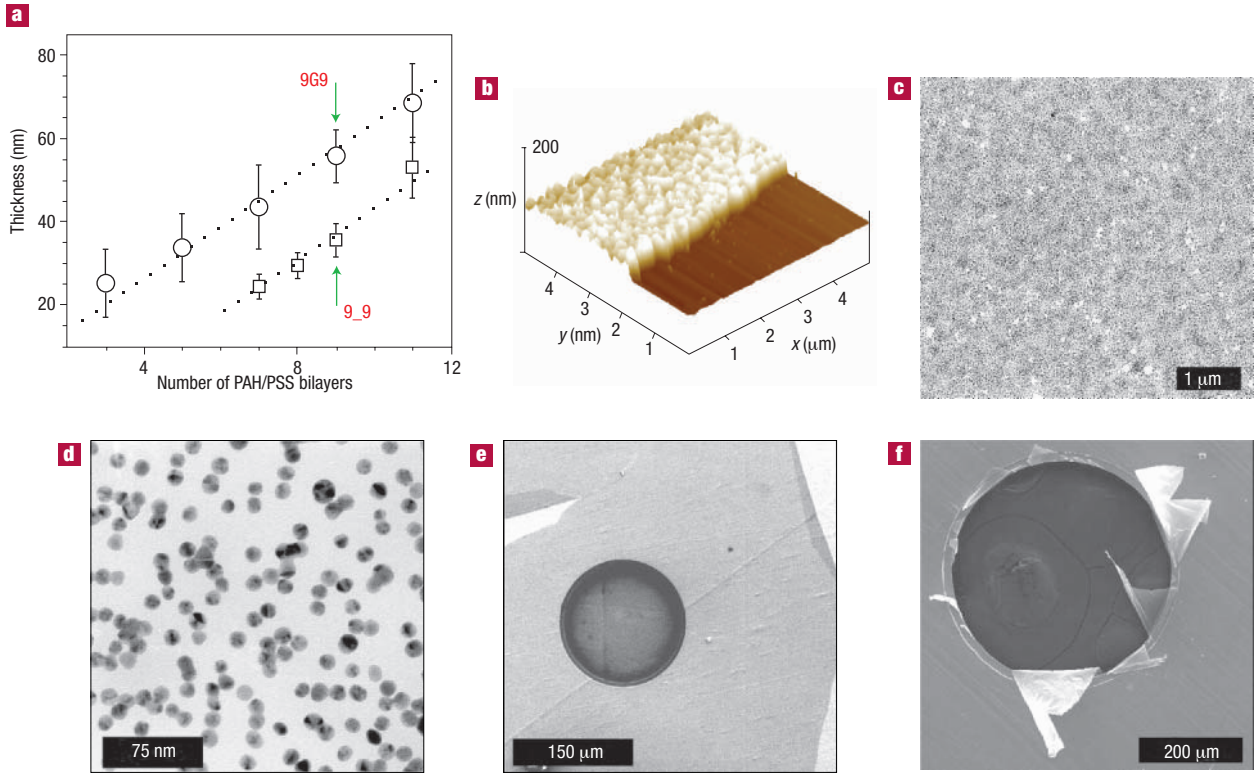

Figure 2 Characterizations of freely suspended nanocomposite membrane containing gold nanoparticles. a, Thickness variation of nGn (with gold nanoparticles; circles — data from ref. 22), and n_n (without gold nanoparticles; squares) membranes with a different number of polymer bilayers. The arrows indicate the membrane selection used for the current study. The error bars are standard deviations. **b**, 3D AFM image of 9G9 membrane edge on a silicon wafer surface. **c**, Large-area TEM micrograph of nanomembrane. **d**, Higher resolution TEM image of freely suspended membrane, which shows isolated gold nanoparticles inside the membrane. **e**, SEM micrograph of 9G9 membrane suspended over the hole with a diameter of 150 μm; the underlying sample holder can be seen as a thin line through the membrane. **f**, SEM image of a broken 9G9 membrane with a hole diameter of 400 μm.

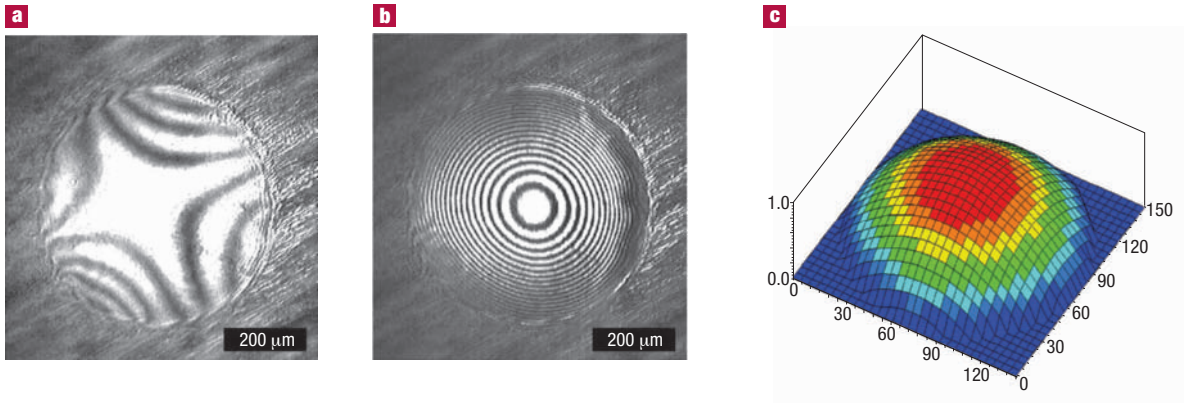

Figure 3 Bulging test of the 600 μm freely suspended nanocomposite membrane monitored by its interference pattern. a, Interference pattern for 9G9 membrane at rest. **b**, Interference pattern for 9G9 membrane with positive pressure applied. **c**, An example of a 3D profile of 150 μm membrane calculated from the interference pattern. All scales are in micrometres.

report. The total membrane thickness can be precisely controlled over a wide range, with a step size of 2.7 nm per polymeric bilayer, by varying the number of bilayers (Fig. 2a). The gold nanoparticles were used to enhance the optical reflection and to control the mechanical properties and sensitivity of the films[22]. The colour of the membranes in solution after release appeared as a light blue, which was caused by a broad absorption peak around 600 nm due to the plasmon resonances of gold nanoparticles (see Supplementary Information)[19].

The surface morphology of SA-LbL nanomembranes is shown in the 3D atomic force microscopy (AFM) image of the edge of the 9G9 nanomembrane on a silicon surface and in a direct transmission electron microscopy (TEM) image of freely suspended membranes (Fig. 2b–d). The membranes were uniform with a microroughness (within 1 μm^2 surface area) below 4 nm for pure polymer membranes and somewhat higher for nanocomposite membranes (8–10 nm). The membranes fabricated without gold nanoparticles showed a lower microroughness and were thinner due to the absence of the gold nanoparticle layer. The packing density of gold nanoparticles in the central layer varied from very low (<2%) to the highest density of 25% (ref. 19). TEM images of the 9G9 membrane showed a uniform large-scale distribution of gold nanoparticles (Fig. 2c) with initial formation of chain-like aggregates visible at high resolution (Fig. 2d). AFM demonstrated that the gold nanoparticles were completely covered by the top polymer bilayers, resulting in a film microstructure as presented in Fig. 1 (ref. 19). No signs of any additional polymer aggregation (for example, crystallites, clusters) have been found for these nanomembranes. Membrane pieces up to 1 cm^2 floated in water after release and were easily transferable onto either silicon or copper substrates having a central hole diameter from 100 μm to 600 μm as can be seen in the SEM image in Fig. 2e. Breaking the membranes resulted in jagged pieces clamped to hole edges (Fig. 2f). Most remarkably, these membranes in a dry state with an overall thickness of 25–70 nm and millimetre lateral dimensions were robust enough to sustain solution treatment during transfer (water and acetone), elevated temperature (heating to 120 °C), high vacuum during TEM and SEM studies, long storage (several months), and repeated mechanical stresses associated with mechanical tests. Although good stability has been demonstrated for some conventional LbL films, the examples reported to date are limited to films deposited onto a solid support as well as to freely suspended films, which are either relatively thick (hundred layers) or relatively small (micrometres) pieces placed in fluid.

Micromechanical behaviour tests were conducted using two different experiments: for larger deflections (micrometres), a bulging test was used where either positive or negative pressure was applied to the freely suspended membrane[23]; tests of nanoscale deflections were measured with AFM. An optical interferometer was used in the bulging test to monitor microscopic deflections of the membrane with a 300 nm resolution (Fig. 3). Variable interference patterns were observed in both a rest state, where the external, noisy environment of the lab caused vibrations large enough to be monitored on the films (Supplementary Information), and in a bulged state, where a series of concentric Newton rings were observed when pressure was applied (Fig. 3a,b). These rings had a very uniform spacing indicating that the deflections of the membranes were spherically shaped, as confirmed in the 3D profile directly obtained from interferometry (Fig. 3c)[24]. Significant elastic deflections, with magnitudes of 20–40 μm, were repeatedly observed as can be seen in a real-time movie taken during the deflections (see Supplementary Information).

Figure 4a,b shows the maximum deflection for freely suspended membranes with different diameters under a variable applied pressure. The membrane's response was clearly nonlinear and consistent with the theoretical prediction for the large elastic deformation of a circular plate clamped to a stiff edge (Supplementary Information)[25]. The experimental data was fit with an appropriate equation having a dominant cubic term, indicating that the films are in the membrane regime where internal stresses control their mechanical behaviour (Fig. 4a,b, and Supplementary Information)[5].

The value of the elastic modulus obtained for 9G9 nanomembranes using these theoretical analyses and fittings was calculated to be within 3–11 GPa (depending on the hole diameter, and testing and fabrication times; Table 1). The specific value (at least three different specimens with the same composition were tested for each membrane diameter) varied within 40% from film to film, illustrating reasonable reproducibility of the fabrication procedure. Within this deviation, the average elastic modulus for all 9G9 membranes fabricated and tested in this study (close to 20) was determined to be 8 ± 3.5 GPa. This is an unprecedented value for nanoscale membranes, and is close to that found for thick (micrometres), traditional LbL films filled with a very significant fraction (close to 30–40% by volume) of very rigid fillers (for example, carbon nanotubes and clay particles)[20,21]. This is even more remarkable considering that the overall volume fraction of gold nanoparticles within the membranes was only about 4%. Moreover, this large value indicates that there are no significant 'weak points' or defects

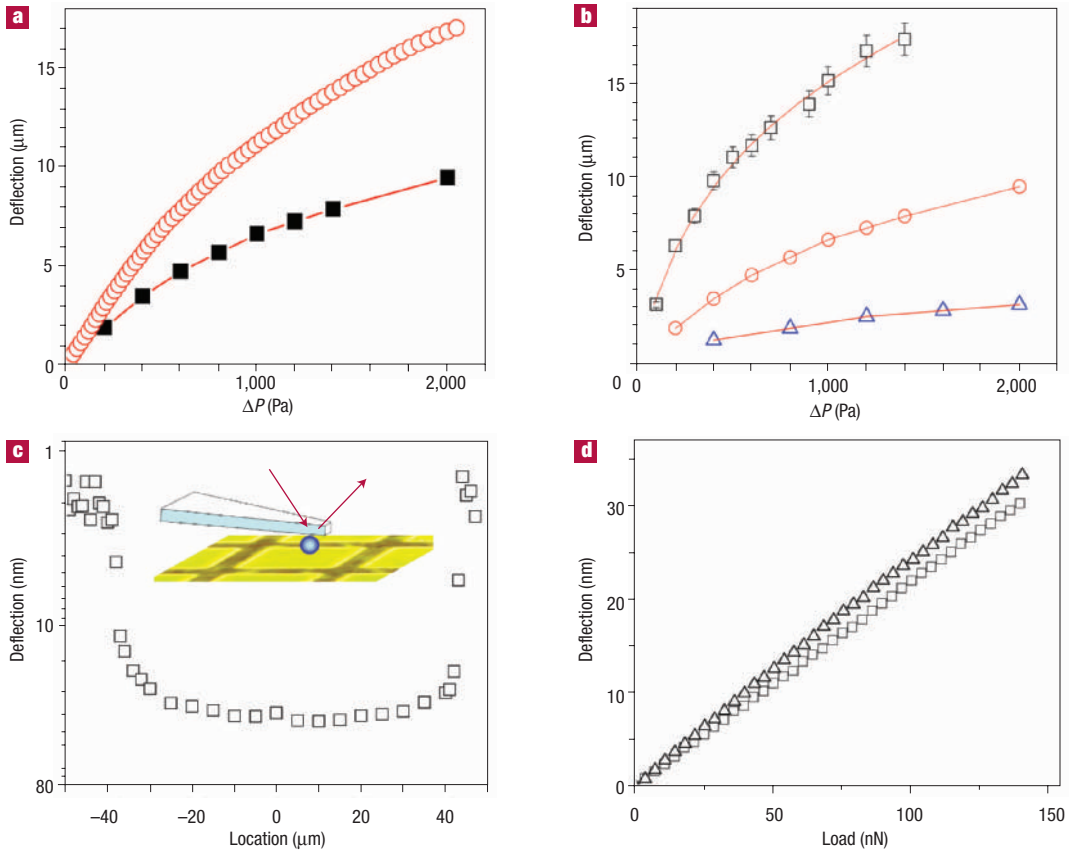

Figure 4 Mechanical testing of membranes. **a**, Deflection of the 9G9 (filled squares) and 9_9 (open circles) membranes (diameter 400 μm) with pressure (*P*). **b**, Deflection of membranes with different diameters: 600 μm (squares; data from ref. 22), 400 μm (circles), and 150 μm (triangles). Solid lines show theoretical fits. Error bars are standard deviations (for circles and triangles, the bars are smaller than the symbols). **c**, Membrane deflection across the TEM grid cells derived from AFM probing of 9G9 membrane. Inset: a cartoon of the experimental setup. **d**, Nanoscale deflection of 9G9 membrane for AFM probing in two different locations.

(cracks, holes, thinning) across these fairly large surface areas (up to 0.4 mm^2) despite their nanoscale thickness of 55 nm. The ultimate strength of these membranes reached 40–100 MPa with the elongation to break approaching 1–2%; both parameters are also exceptional for nanoscale films.

The micromechanical properties can be controlled by varying the composition of the nanocomposite membranes. Decreasing the content of gold nanoparticles resulted in significantly decreasing the elastic modulus (Table 1), which indicates the filler toughening mechanism associated with gold nanoparticles embedded in these films[26]. In fact, complete removal of gold nanoparticles from the central layer (the 9_9 membrane) resulted in a much more compliant behaviour of this purely polymeric multilayered membrane, as presented in the comparison of deflection-pressure data in Fig. 4a. The elastic modulus of this membrane with 18 PSS-PAH bilayers became much lower, close to 1 GPa (Table 1); however, this is consistent with the value predicted from the composite material model suggested by Takayanagi, in which the gold nanoparticles were completely removed[26]. This high value of the elastic modulus for PSS-PAH membranes freely suspended in air was independently confirmed by careful AFM indentation for LbL surface areas located on the silicon surface. These measurements have been conducted according to the routine that takes into account the substrate influence and adhesive contribution[27,28]. The value of the elastic modulus of about 1 GPa indicates the 'near-glassy' state of dry LbL membranes without gold nanoparticles. The elastic modulus of PSS-PAH layers being in the glassy state (glass-transition temperature for both polymers is in the range of 160–190 °C, ref. 29) was measured[20] to be close to 2.5 GPa and this value should drop to tens of MPas after transition to the rubbery state caused by either elevated temperature or partial swelling in appropriate solvent.

The glassy state of the LbL films studied here can be apparently related to their dry, solvent-free state and the small strain used in our studies (usually well below 1%). It is worth noting that the mechanical properties of polyelectrolyte multilayer films have been already investigated with different methods such as applying osmotic pressure to microcapsules, AFM nanoindentation, interferometry and direct compression with AFM tip[30–34]. Some of these studies indicated the glassy state of the LbL films with the elastic modulus close to that reported here (0.5–2 GPa) with others claiming the elastomeric behaviour of the LbL films with much lower elastic modulus within 0.1–200 MPa. As has been pointed out in an excellent review on this subject[35], the dramatic decrease of the apparent elastic modulus of the LbL membranes can be associated with a fluidic environment resulting in partial membrane swelling and large deformations—all circumstances absent in our study.

It is worth noting that polyelectrolyte LbL membranes adsorb water—a good solvent for polymer components—a phenomenon that

can act as a plasticizer and influence the film's properties[21,35,36]. As stated above, conventional ultrathin LbL films fabricated here were readily broken into smaller pieces, making it impossible to collect them with a holey substrate whereas SA-LbL films kept their integrity during the demanding transfer procedure. Apparently, the presence of some 'weak points' expected for very thin conventional LbL membranes compromised their large-scale integrity. As known, much thicker (>300–500 nm thickness) and much smaller (below 40 μm microcapsules) multilayers obtained with conventional LbL assembly show a good environmental stability[35]. However, an outstanding stability of both very thin (25–70 nm) and very large (millimetres–centimetres) membranes is observed only for the SA-LbL membranes reported here. It is worth noting that even for these SA-LbL films, less successful transfer was observed under conditions of higher humidity and after thermal treatment. Within a normal variation of humidity (25–50% in our cleanroom), the elastic properties of the films fluctuated 30–40% from the average, as measured at different times in the span of half a year. On the other hand, these membranes sustained several hours of treatment at elevated temperature (120 °C), showing modest decrease in the elastic modulus. These responses to environmental changes however, are still much less dramatic than that observed for conventional LbL films.

The high stability of ultrathin SA-LbL membranes is in contrast to multilayered films of the same number of layers obtained by conventional LbL assembly fabricated here for comparative purposes. These conventional films floating in acetone were so fragile that they rarely could be transferred to solid substrates, and were easily damaged during the transfer procedure. In the rare case when transfer to a solid substrate was successful, the conventional LbL film broke into small pieces while drying. In contrast, both gold-containing SA-LbL membranes kept their integrity in both acetone and water, remained intact on transfer to a solid substrate, sustained multiple, significant deflections, high vacuum in SEM and TEM, and survived random vibrations in a noisy environment over a period of many months. Moreover, even the purely polymeric membranes with a total thickness of about 35 nm showed excellent stability. Apparently, both the nanocomposite, multilayered nature of the SA-LbL membranes with a central nanoparticle-containing layer sandwiched between polymer outer layers, and their peculiar microstructure resulting from spin-assisted assembly, are critically important for the realization of these outstanding properties.

To evaluate the sensitivity limits of 9G9 membranes suspended over a copper TEM grid (a single cell dimension of 85 × 85 μm^2), the nanoscale deformation behaviour was tested with a colloidal AFM probe (used to prevent local rupture), as demonstrated in Fig. 4c. Membrane deflections under a point load of 150 nN reached 30 nm. An analysis of the loading behaviour (deflection versus normal load) far from the edges revealed a uniform response across the membrane (compare data for two locations in Fig. 4d)[5,37]. The linear loading behaviour indicated the bending mechanism of deformation under low forces and deflections smaller than the total thickness of the membrane[5]. The minimum detected membrane deflection, about 2 nm, was observed under a normal load of 4 nN. The bending stiffness of 9G9 freely suspended membrane was estimated to be about 2 N m^{-1}, which is significantly higher than the bending parameters reported for polymer multilayers of microcapsules submerged in fluid[31].

Therefore, the deflection measurements demonstrate that these films are responsive to both nanoscale (1–30 nm) and microscale (30–40 μm) deflections which makes them unique multi-length-scale membranes. A measure of the ratio of the highest to the lowest detectable pressures gave a value of this dynamic range of about 10^8 for these nanomembranes. This far exceeds any known dynamic range for inorganic-based membranes (usually below 10^5) and silicon microcantilevers. Moreover, tests of the resonant properties of these nanomembranes revealed their low damping, stable resonance at a resonant frequency of about 100 kHz with an amplitude of 25 nm for a 400 μm diameter, 9G9 membrane, as will be discussed in detail elsewhere. This makes these membranes excellent candidates for resonance, high-speed readout arrays used in un-cooled thermal and acoustic imaging sensors.

The most outstanding result is presented in Fig. 5, which displays the sensitivity data (membrane deflection versus pressure) for a 9G9 membrane with a 600 μm diameter obtained from bulging experiments (two independent bulging measurements are included) for large deflections and AFM experiments for nanoscale deflections (extrapolated from point to distributed pressure). The two independent, linear extrapolations of these data in log–log coordinates are justified by theoretically predicted different slopes in the membrane regime (slope of 3 for large deflections, d, $d>>h$, where h is the thickness) and the bending mode (slope of 1 for small deflections, $d<h$) with $d = h = 55$ nm being a natural boundary (see black arrow in Fig. 5).

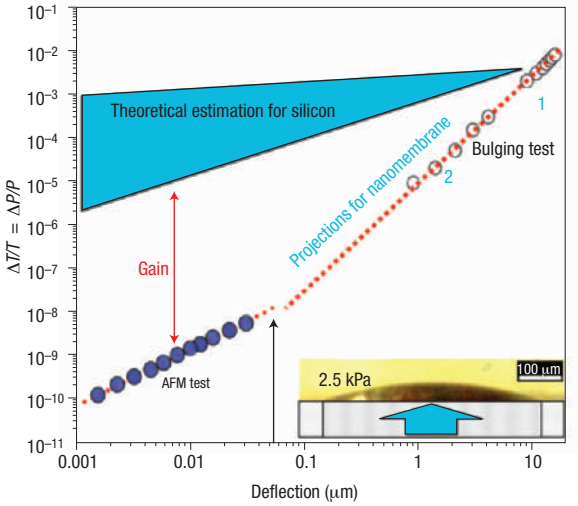

Figure 5 Pressure–temperature sensitivity of freely suspended 9G9 membrane of 600 μm diameter in comparison with a silicon membrane of the same diameter. The relative variation of pressure is equivalent to relative variation of temperature (T) for the isochoric regime. The results of two independent bulging tests (1 and 2) (open circles) for high deflections and AFM distributed-pressure results for nanoscale deflections (filled circles) are used to estimate the overall behaviour. The black arrow shows the membrane thickness. The insert shows a side-view of a deflected membrane.

Table 1 Mechanical parameters for different freely suspended nanomembranes calculated from bulging tests.

Membrane type and gold content	Fabrication method	Membrane diameter (μm)	Elastic modulus (GPa)
9G9, 3.9%	SA-LbL	600	6.6 ± 2.3
9G9, 3.9%	SA-LbL	400	9.6 ± 2.5
9G9, 3.9%	SA-LbL	150	5.7 ± 3.0
9G9, 0.5%	SA-LbL	400	4.3 ± 2
9_9, 0%	SA-LbL	400	1.5 ± 1
9G9, 4%	LbL	N/A *	N/A *

*Film was broken in small pieces after release, which are non-transferable to a holey substrate

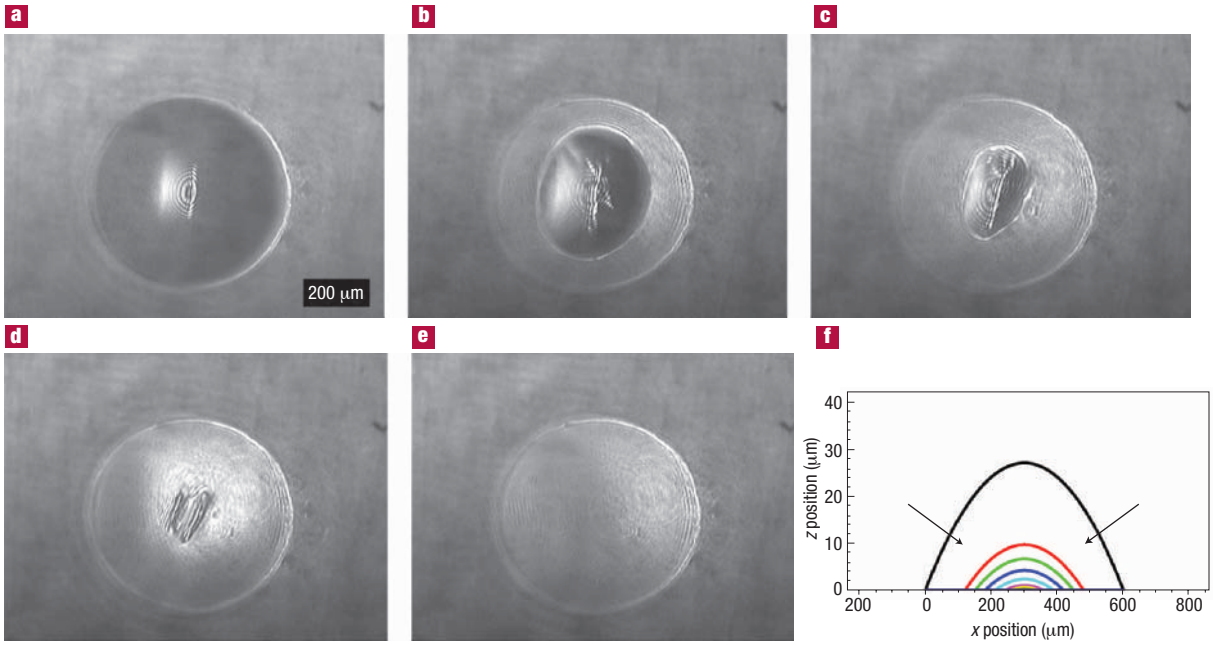

Figure 6 Autorecovery of the freely suspended 9G9 membrane subjected to high pressure and long loading time. a, Optical interference pattern for the membrane under high-pressure (4 kPa). **b–e**, The membrane shape response after sudden pressure release demonstrating gradual recovery to the flat state as determined by the disappearance of the overstretched central portion (images are presented at every two seconds). **f**, A series of corresponding membrane cross-sections obtained every second with arrows showing the direction of the recovery of the central portion. All images here are on the same scale.

The expected sensitivity range of a silicon membrane, evaluated from data for microthermal sensors[7] extrapolated to a diameter of 600 μm, is presented for comparison. As obvious from this plot, the compliant, nanocomposite membranes introduced here possess outstanding sensitivity three to four orders of magnitude higher than that seen for the silicon membrane of the same diameter. This value far exceeds sensitivity reached in uncooled thermal sensors based on rigid materials reported to date[1]. A theoretical temperature sensitivity well below 1 mK, and an acoustic sensitivity of an order of magnitude below the threshold of human hearing, were estimated for 200 μm diameter 9G9 membranes.

An even more remarkable and unexpected result on the extreme elasticity and recovery ability of the freely suspended SA-LbL membranes was obtained while pushing the limits of their mechanical stability. First, as expected, the viscoelastic contribution became obvious for high applied pressures (close to the ultimate strength) and loading times exceeding 20 seconds. When the pressure on the membrane was released, the film did relax to its initial state, as demonstrated in Fig. 6 (see Supplementary Information for the corresponding real-time movie). Interestingly, the membrane initially returned to the original state only along the edges, while the central portion retained an asymmetric bulged shape of about 300 μm in diameter (Fig. 6b). The film appeared permanently damaged with a plastically deformed centre. However, after further relaxation, the film gradually reduced its jammed central part and completed restoration to its initial flat state. Although the analysis of these over-stretched membranes immediately after relaxation showed some decrease in the elastic modulus, a longer relaxation period (hours) led to a complete restoration of the initial micromechanical properties. To the best of our knowledge, an autorecovery phenomenon of this type has never been reported before and constitutes a novel mechanism for self-healing of composite materials different from recently reported[38]. We believe that this autorecovery mechanism can serve as a safeguard against the event of over-stretching the nanoscale membrane, providing a fast recovery path and high stability for dynamic properties, thus facilitating a long life. In fact, the shelf life of the nanomembranes stored in a noisy environment exceeds six months despite continuous membrane fluctuations.

Although complete understanding of the underlying molecular mechanisms requires further in-depth studies, here we suggest that these films' outstanding sensitivity and recovery abilities are caused by the peculiar multilayered structure of the nanocomposite membranes combined with a high level of spreading of macromolecular chains in the plane of the films and over the metal nanoparticles (Fig. 1). In-plane spreading of random polymer chains within thin monolayers is well known for conventional LbL films[39]. However, the enhanced in-plane spreading should be caused by high shear forces during radial solution flow in the course of spin casting, as has been reported for flexible macromolecular chains similar to those used in this work[40,41]. Moreover, it has been suggested that the SA-LbL technique accelerates the realignment of polymer chains, resulting in dense packing, possible radial orientation, and additional, mechanically induced entanglements between polymer chains, which is a critical strengthening mechanism[42,43]. The presence of a dense network of weak, sacrificial bonds between polyelectrolyte layers with oppositely charged groups that are capable of regrouping and restoring the mechanical properties after pressure is released is another key factor in the mechanical stability of these membranes[44]. This mechanism is thought to be responsible for the outstanding mechanical properties seen in biomimetic LbL films composed of polymer chains and clay flakes[21,44].

In the case of freely suspended membranes, the presence of significant pre-stretching can be suggested as an additional reason for the outstanding micromechanical properties and unusual recovery phenomenon. The pre-stretching phenomenon, where residual stresses reaching several MPa, is observed for freely suspended membranes and is a commonly seen phenomenon in thin polymer films, and is

attributed to their shrinking while drying after being transferred to a solid substrate[45]. The network of mechanically induced entanglements, sacrificial bondings, and significant pre-stretching are all factors that significantly enhance the tendency of the film to restore the polymer molecules to a coiled conformation state after being stretched under stress. These factors make the mechanical behaviour observed here similar to that reported for layered LbL biocomposites (for example, bones, nacres) as well as their biomimetic multilayered analogues[44].

In conclusion, we fabricated freely suspended, nanocomposite, organic–inorganic membranes using a polymer–nanoparticle SA-LbL technique, which resulted in films with record stability and sensitive properties, far surpassing any membrane-based sensors reported to date. These properties make the films unique candidates for a new generation of membrane-based, acoustic, pressure, chemical, and temperature micro-array sensors with superior sensitivity, tremendous dynamic range, and a built-in autorecovery mechanism. We have also demonstrated that it is possible to overcome the current problems associated with conventional, diffusion-controlled assembly and fabricate truly nanoscale, compliant, nanocomposite films with thicknesses of tens of nanometres and large-scale lateral dimensions. These films are not only capable of withstanding the transfer procedure and their own weight in a freely suspended state, but are extremely strong, robust, have a long life, are highly sensitive, and show unprecedent ability to recover. Finally, the fabrication of SA-LbL films is also a much more time-efficient technique than conventional LbL assembly (for example, less than an hour instead of the usual 10 hours for the fabrication of a 9G9 membrane). This provides a way to efficiently fabricate films having a large number of layers if needed, and design more complex superstructures. Recent examples of fabricating patterned and free-standing organic–inorganic sensors by using LbL assembly show a wide variety of prospective applications[46,47].

METHODS

MATERIALS AND CHEMICALS

PSS (M_W = 70,000), and PAH (M_W = 65,000) were purchased from Aldrich and used as received. Ultra pure water was obtained with a Nanopure system (resistivity 18 MΩ cm). Silicon wafers of the {100} orientation with one side polished were cut to a typical size 10 × 20 mm and were then cleaned in fresh piranha solution (1:3 (v/v) H_2O_2/H_2SO_4).

SYNTHESIS OF GOLD NANOPARTICLES

Gold nanoparticles with the average diameter of 12.7 ± 1.2 nm were prepared according to a known procedure[48] and characterized in detail elsewhere[19]. Initially, 5 ml of a 1% sodium citrate solution was injected into 50 ml of a boiling 1 mM $HAuCl_4$ solution. The solution was kept boiling for 10 minutes and cooled with continuously stirring. Fresh gold nanoparticle solution was used.

FABRICATION OF FREELY SUSPENDED MEMBRANES

A sacrificial cellulose acetate (CA) layer was spin coated on the freshly cleaned silicon substrate. A droplet (150 µl) of 1% CA acetone solution was placed on the silicon substrate and rotated for 20 s with a 3,000-r.p.m. rotation speed. The multilayer polymer films (general formula: $(PAH/PSS)_n PAH/Au/(PAH/PSS)_n/PAH)$) with different thicknesses were fabricated using SA-LbL method. A 150 µL droplet of 0.2% PAH solution was dropped on the substrate and rotated for 20 s with a 3,000-r.p.m. rotation speed. The substrate was rinsed twice with Nanopure water and dried while spinning for 30 s. In the same manner, 0.2% PSS solution was deposited. This procedure was repeated until the needed number of polymer bilayers, *n*, was achieved. To form the central layer, a 150 µl droplet of gold nanoparticle solution was dropped on the substrate and was left for 30 minutes. The substrate was then rinsed twice with Nanopure water and the same number of polymer bilayers, *n*, was again deposited. Acetone solution was used to dissolve the sacrificial CA layer and resulted in the release of the membrane. The membranes were next transferred to Nanopure water where they could then be picked up with either a highly polished copper plate with a single micromachined hole in its centre, a clean silicon wafer, or a copper TEM grid.

AFM MEASUREMENTS

AFM topographical and phase images were collected using a Dimension 3000 AFM microscope (Digital Instruments) in the tapping mode according to the usual procedure adapted in our laboratory for ultrathin polymer films[49]. The radii of silicon tips were in range of 20-40 nm, as calculated from the profile of a reference gold nanoparticle standard. AFM images were obtained with scan sizes from ranging from 1 µm to 20 µm. To obtain a film thickness, the freely suspended membrane was picked up on the silicon wafer and its edge area was scanned.

POINT-LOAD AFM MEASUREMENTS

Point-load measurements were preformed for the freely suspended membrane on a copper grid with a 200 mesh (cell size of 85 µm × 85 µm). Silicon cantilevers used for this testing had a spring constant of 14.0 ± 2.8 N m^{-1}, a value measured independently[50]. Cantilevers with 2.5 µm glass microspheres attached to their end were used for these experiments.

TEM AND SEM IMAGING

A Phillips CM30 electron microscopy with a LaB_6 filament was operated at 300 kV and used for TEM study. The morphology of the membranes was investigated with JSM-6060LV scanning electron microscope.

BULGING TEST

The bulging test was conducted by applying a hydrostatic pressure to one side of a membrane that covered a copper plate having a single hole. The hole diameter varied from 100 µm to 600 µm. The applied pressure was controlled with a precision of ±5 Pa by measuring the height difference of a water-filled, U-shaped glass column. The membrane deflection was measured using a custom-built interference optical set-up with a helium–neon laser. Optical images with a variable number of Newton rings were recorded by a CCD camera. The deflection of the top of the membrane was calculated by determining the average spacing between fringes from 1D Fourier transforms. The 3D membrane profile was calculated from the interference pattern using the Quick Fringe software package (Diffraction Limited).

Received 10 February 2004; accepted 26 July 2004; published 26 September 2004.

References

1. Rogalski, A. Infrared detectors: status and trends. *Progr. Quant. Electron.* **27,** 59–210 (2003).
2. Defay, E., Millon, C., Malhaire, C. & Barbier, D. PZT thin films integration for the realization of a high sensitivity pressure microsensor based on a vibrating membrane. *Sens. Actuat. A* **99,** 64–67 (2002).
3. Hedrich, F., Billat, S. & Lang, W. Structuring of membrane sensors using sacrificial porous silicon. *Sens. Actuat. A* **84,** 315–323 (2000).
4. Davidson, J. L., Wur, D. R., Kang, W. P., Kinser, D. L. & Kerns, D. V. Polycrystalline diamond pressure microsensor. *Diam. Related Mater.* **5,** 86–92 (1996).
5. Timoshenko, S. & Woinowsky-Krieger, S. *Theory of Plates and Shells* (McGraw-Hill, New York, 1959).
6. Chévrier, J. B., Baert, K. & Slater, T. An infrared pneumatic detector made by micromachining technology. *J. Micromech. Microeng.* **5,** 193–195 (1995).
7. Yamashita, K., Murata, A. & Okuyama, M. Miniaturized infrared sensor using silicon diaphragm based on Golay cell. *Sens. Actuat. A* **66,** 29–32 (1998).
8. Lee, D. R. *et al.* X-ray scattering from freestanding polymer films with geometrically curved surfaces. *Phys. Rev. Lett.* **90,** 185503 (2003).
9. Cuvillier, N., Petkova, V., Nedyalkov, M., Millet, F. & Benattar, J.-J. Protein insertion within a biological freestanding film. *Physica B* **283,** 1–5 (2000).
10. Yablonskii, S. V., Nakano, K., Mikhailov, A. S., Ozaki, M. & Yoshino K. Thermal photodetector using freely suspended liquid-crystal films. *Jpn J. Appl. Phys.* **42,** 198–201 (2003).
11. Goedel, W. A. & Heger, R. Elastomeric suspended membranes generated via Langmuir-Blodgett transfer. *Langmuir* **14,** 3470–3474 (1998).
12. Kotov, N. A. Ordered layered assemblies of nanoparticles. *Mater. Res. Soc. Bull.* **26,** 992–997 (2001).
13. Decher, G. & Schlenoff, J. B. (eds) *Multilayer Thin Films* (Wiley-VCH, Weinheim, 2003).
14. Decher, G. Fuzzy nanoassemblies: toward layered polymeric multicomposites. *Science* **277,** 1232–1237 (1997).
15. Lvov, Y., Decher, G. & Möhwald, H. Assembly, structural characterization, and thermal behavior of layer-by-layer deposited ultrathin films of poly(vinyl sulfate) and poly(allylamine). *Langmuir* **9,** 481–486 (1993).
16. Tsukruk, V. V. Dendritic macromolecules at interfaces. *Adv. Mater.* **10,** 253–257 (1998).
17. Cho, J., Char, K., Hong, J.-D. & Lee, K.-B. Fabrication of highly ordered multilayer films using a spin self-assembly method. *Adv. Mater.* **13,** 1076–1078 (2001).
18. Chiarelli, P. A. *et al.* Controlled fabrication of polyelectrolyte multilayer thin films using spin-assembly. *Adv. Mater.* **13,** 1167–1171 (2001).
19. Jiang, C., Markutsya S. & Tsukruk, V. V. Collective and individual plasmon resonances in nanoparticle films obtained by spin-assisted layer-by-layer assembly. *Langmuir* **20,** 882–890 (2004).
20. Mamedov, A. A. & Kotov, N. A. Free-standing layer-by-layer assembled films of magnetite nanoparticles. *Langmuir* **16,** 5530–5533 (2000).
21. Mamedov, A. A. *et al.* Molecular design of strong single-wall carbon nanotube/polyelectrolyte multilayer composites. *Nature Mater.* **l,** 190–194 (2002).
22. Jiang, C., Markutsya, S. & Tsukruk, V. V. Compliant, robust, and truly nanoscale free-standing multilayer films fabricated using spin-assisted layer-by-layer assembly. *Adv. Mater.* **16,** 157–161 (2004).
23. Neugebauer, C. A., Newkirk, J. B. & Vermilyea, D. A. *Structure and Properties of Thin Solid Films* (Wiley, New York, 1959).
24. Jones, R. & Wykes, C. *Holographic and Speckle Interferometry: A Discussion of the Theory, Practice and Application of the Techniques* (Cambridge Univ. Press, New York, 1983).
25. Poilane, C., Delobelle, P., Lexcellent, C., Hayashi, S. & Tobushi, H. Analysis of the mechanical behavior of shape memory polymer membranes by nanoindentation, bulging and point membrane deflection tests. *Thin Solid Films* **379,** 156–165 (2000).
26. Sperling, L. H. *Polymeric Multicomponent Materials* 37 (Wiley, New York, 1997).
27. Kovalev, A., Shulha, H., LeMieux, M., Myshkin, N. & Tsukruk V. V. Nanomechanical probing of layered nanoscale polymer films with atomic force microscopy. *J. Mater. Res.* **19,** 716–728 (2004).
28. Tsukruk, V. V., Shulha, H. & Zhai X. Nanoscale stiffness of individual dendritic molecules and their aggregates. *Appl. Phys. Lett.* **82,** 907–909 (2003).
29 Yamagata, Y. & Shiratori, S. Evaluation of electrical characteristics of the layer-by-layer self-assembled films after the various annealing temperatures. *Thin Solid Films* **438–439,** 238–242 (2003).
30. Gao, C., Leporatti, S., Moya, S., Donath, E. & Möhwald, H. Stability and mechanical properties of polyelectrolyte capsules obtained by stepwise assembly of PSS and PAH onto melamine resin particles. *Langmuir* **17,** 3491–3495 (2001).
31. Dubreuil, F., Elsner, N. & Fery, A. Elastic properties of polyelectrolyte capsules studied by atomic-force microscopy and RICM. *Eur. Phys. J. E* **12,** 215–221 (2003).
32. Lulevich, V. V., Radtchenko, I. L., Sukhorukov, G. B. & Vinogradova, O. I. Deformation properties of nonadhesive polyelectrolyte microcapsules studied with atomic force microscope. *J. Phys. Chem.* **107,** 2735–2740 (2003).
33. Vinogradova, O. I., Andrienko, D., Lulevich, V. V., Nordschild, S. & Sukhorukov, G. B. Young's

modulus of polyelectrolyte multilayers from microcapsule swelling. *Macromolecules* **37,** 1113–1117 (2004).
34. Mermut, O., Lefebvre, J., Gray, D. G. & Barrett, C. J. Structural and mechanical properties of polyelectrolyte multilayer films studied by AFM. *Macromolecules* **36,** 8819–8824 (2003).
35. Fery, A., Dubreuil, F. & Möhwald, H. Mechanics of artificial microscapsules. *New J. Phys.* **6,** 18 (2004).
36. Vogt, B. D., Soles, C. L., Lee, H., Lin, E. K. & Wu, W. Moisture absorption and absorption kinetics in polyelectrolyte films: influence on film thickness. *Langmuir* **20,** 1453–1458 (2004).
37. Vlassak, J. J. & Nix, W. D. A new bulge test technique for the determination of Young's modulus and Poisson's ratio of thin films. *J. Mater. Res.* **7,** 3242–3249 (1992).
38. White, S. R. *et al.* Autonomic healing of polymer composites. *Nature* **409,** 794–797 (2001).
39. Tsukruk, V. V. *et al.* Electrostatic deposition of polyionic mono/bilayers on charged surfaces. *Macromolecules* **30,** 6615–6625 (1997).
40. Prest, W. M. & Luca, D. J. The origin of the optical anisotropy of solvent cast polymer films. *J. Appl. Phys.* **50,** 6067–6071 (1979).
41. Law, C. W., Wong, K. S., Yang, Z., Horsburgh, K. S. & Monkman A. P. Observation of in-plane optical anisotropy of spin-cast rigid-rod electroluminescent polymer films. *Appl. Phys. Lett.* **76,** 1416–1418 (2000).
42. Chiarelli, P. A. *et al.* Polyelectrolyte spin-assembly. *Langmuir* **18,** 168–173 (2002).
43. Lee, S.-S., Lee, K.-B. & Hong, J.-D. Evidence for spin coating electrostatic self-assembly of polyelectrolytes. *Langmuir* **19,** 7592–7596 (2003).
44. Tang, Z., Kotov, N., Magonov, S. & Ozturk, B. Nanostructured artificial nacre. *Nature Mater.* **2,** 413–418 (2003).
45. Francis, L. F., McCormick, A. V., Vaessen, D. M. & Payne, J. A. Development and measurement of stress in polymer coatings. *J. Mater. Sci.* **37,** 4717–4731 (2002).
46. Hua, T., Cui, T. & Lvov, Yu. M. Ultrathin cantilevers based on polymer-ceramic nanocomposite assembled through LbL adsorption. *Nano Lett.* **4,** 823–825 (2004).
47. Zheng, H., Lee, I., Rubner, M. & Hammond, P. Controlled cluster size in patterned particle arrays via directed adsorption on confined surfaces. *Adv. Mater.* **14,** 573–577 (2002).
48. Grabar, K. C., Freeman, R. G., Hommer, M. B. & Natan, M. J. Preparation and characterization of Au colloid monolayers. *Anal. Chem.* **67,** 735–743 (1995).
49. Tsukruk, V. V. Scanning probe microscopy of polymer surfaces. *Rubber Chem. Technol.* **70,** 430–475 (1997).
50. Hazel, J. L. & Tsukruk V. V. Spring constants of composite ceramic/gold cantilevers for scanning probe microscopy. *Thin Solid Films* **339,** 249–257 (1999).

Acknowledgements

This work was supported by the National Science Foundation, CTS-0210005 Grant and the Air Force Office of Science Research, F496200210205 Contract. The authors thank X. Tan and A. Bastawros, Iowa State University and M. R. Beggley, University of Virginia for valuable discussion, F. Laabs and M. Kramer, the Department of Energy Ames Laboratory for access to TEM and assistance with TEM studies, and B. Rybak for assistance with SEM studies.
Correspondence and requests for materials should be addressed to V.V.T.
Supplementary Information accompanies the paper on www.nature.com/naturematerials

Competing Interests statement

The authors declare that they have no competing financial interests.